The local concept to assess weldment with help of nano-indentation and FEM simulation

Jie Fang, Huang Yuan*

Department of Mechanical Engineering, University of Wuppertal, Germany
* Corresponding author: h.yuan@uni-wuppertal.de

Abstract In this work the local mechanical behavior and fatigue resistance of the welding material were investigated with help of nano-indentation. By assuming a power-law strain hardening, the elastoplastic properties of the welding joint material were identified from inverse nano-indentation analysis with help of finite element simulation. With the known mechanical property of the weldment the fatigue should be described by the local stresses and strains. A critical plane based Cruse-Meyer model was introduced to predict the fatigue life of weldment. The predictions agree with experiments. Combined with critical distance concept the local fatigue life model was extended to predict fatigue life of holed specimens. The present work attempted to establish more reliable and more accurate a local fatigue and damage description of the weldment for engineering structures.

Keywords Nano-indentation, Weldment, Notched Fatigue, Extended Cruse-Meyer Model, Critical Distance Method.

1. Introduction

With the development of aero engines, welding has been widely used to manufacture aircraft engine components for better performance. Many welding methods such as tungsten inert gas welding, plasma welding, electron beam welding (EBW), diffusion welding and friction welding have been developed and used for the welding of Inconel alloys. Compared with traditional fusion welding technology, the electron beam welding has a narrow heat-affected zone with little distortion and low residual stresses [1]. Very high quality welds can be made during the manufacturing of complex components. Being a fusion welding process, the weld joint of EBW has significantly different properties to the base material.

Nano-indentation is a method to extract the mechanical properties of materials from load-displacement measurements [2]. Hardness and Young's modulus can be obtained from the indentation curve based on the Oliver and Pharr method [3] to characterize micromechanical behavior of material. More depth knowledge about mechanical properties can be gained with help of finite element simulation through an inverse analysis procedure [4]. The local mechanical property of the weldment makes it possible to establish fatigue life prediction based on local stress and strain variations.

In design of a gas turbine engine, notches and holes are not avoidable, for instance, in disks and blades, which cause local stress concentrations and lead to significant reduction in fatigue life. In industrial design the stress concentration factor, K_t, is often used to characterize the stress concentration. Under cyclic loading, the fatigue notch factor, K_f, is introduced to describe the change of fatigue strength [5]. Notched fatigue strength depends not only on K_t, but also on the stress gradient which relates the material volume with the high stress. Peterson [6] and Neuber [7] try to describe the difference between K_f with K_t through empirical relations. Siebel and Stieler [8] proposed using the stress gradient at a notch root for evaluation of the notch effect. Taylor developed the former works and proposed the theory of critical distance (TCD) [9]. Susmel and Talyor [10,11,12] successfully extended the TCD to the LCF regime. By employing an elasto-plastic critical plane approach, the TCD is extended to consider multi-axial fatigue.

In this work the stress-strain relation and tensile fatigue resistance of the EB weld joints are investigated. This work aims to develop a method to determine the local elastoplastic properties of

weldment material, and to predict fatigue life of weldment with stress concentrations. The local elastoplastic properties of weldment material are derived from inverse nano-indentation analysis. From FEM simulation the nominal stress-strain curve of weld joint is obtained and compared with the monotonic tensile curve. A critical plane method based Cruse-Meyer model is applied to predict the fatigue life of weldment. Combined with critical distance method center holed specimen fatigue life was calculated and compared with the experiment.

2. Experiments

Inconel 718 is a precipitation-hardenable nickel-chromium alloy, contains large amount of iron, niobium and molybdenum. Due to the outstanding combination of tensile strength, high temperature creep strength and high resistance to fatigue, this alloy is widely used in the high pressure compressor and turbine discs of commercial and military aero engines and recommended for using up to 650°C [13]. The composition of the alloy is given in Table 1. After electron beam welding process, post-weld heat treatment was applied. Specimens were cut from the welded joint material with weldment in the center of the specimen. Surface of raw specimens was removed and machined to a thickness of 4mm, resulting weldment shape changing from bell shape to trapezoid shape. Fig. 1 shows the geometry of the holed specimen. All tests were carried out at the room temperature.

Table 1. Chemistry of Inconel 718

	Ni	Fe	Cr	Mo	Nb	Al	Ti	C
Weight%	balance	18.5	19.0	3.0	5.1	0.5	0.9	0.04

2.1 Tensile and Fatigue Test

Monotonic tensile test was conducted at strain rate 10^{-4}/s. Cracks originated from the weldment. Tensile failure occurred in the center of weldment, while shear failure occurred in the outer side. Yield stress and ultimate tensile stress of weld joint were lower than base material. Fatigue tests were performed under stress control at stress ratio, R = -1, 0.1. The fatigue life was defined as the number of cycles when a specimen was completely separated.

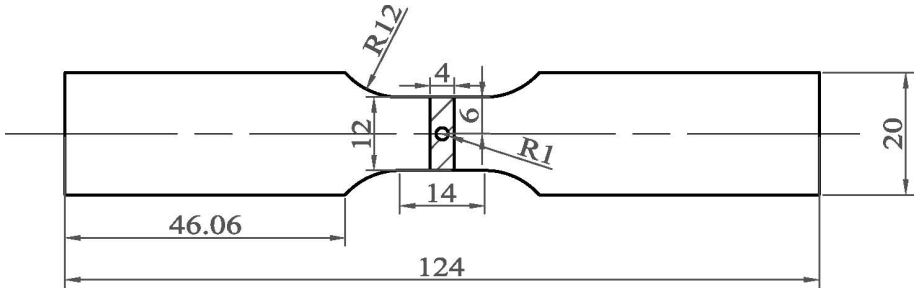

Figure 1. Geometry of center holed EB welded specimen.

2.2 Macroscopic and microscopic observation of weld joint

Fig. 2a shows the fusion region of EB welding joint by macroscopic observation. The fusion zone is quite narrow, formed in 2-4mm width. The fusion boundary is clearly evident. No significant heat affected zone can be seen. The evolution of microstructure from the base material to the fusion zone can be clearly recognized. Fig. 2b shows a microscopic observation near fusion boundary. Large

grain size gradient between the weldment (left side) and the base material (right side) is clearly seen. The average grain size of the base material is about 50μm. In the fusion zone, the microstructure is composed of columnar grains, while original grain structure no longer exits. The columnar grains orient perpendicular to the direction of the radial fusion boundary. The grain differences between fusion zone and base material would lead to different mechanical behavior.

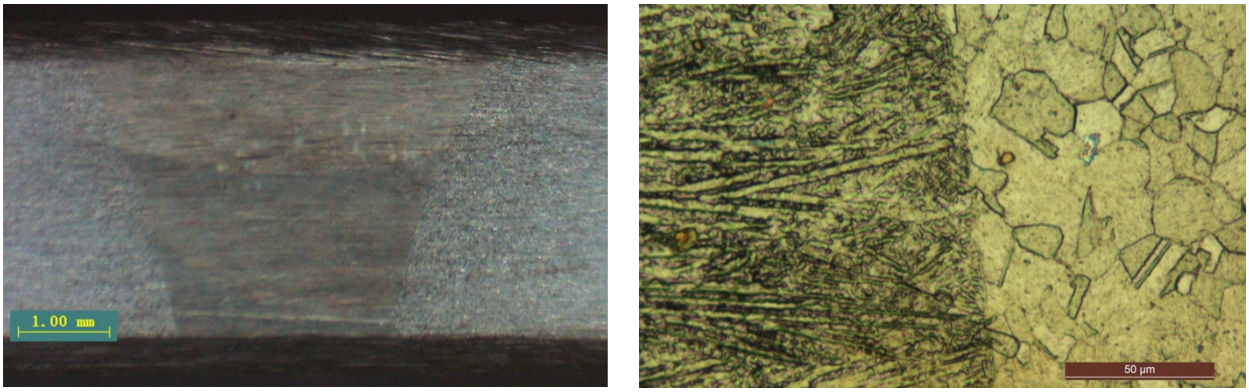

(a) (b)

Figure 2. (a) Macroscopic view of the weld joint and (b) Microstructure of the fusion boundary.

2.3 Nano-indentation test

For nano-indentation test, a nano indenter G200 from Agilent Technologies was used. The depth resolution is 0.01nm and the force resolution is 50nN. Berkovich indenter was used for the identation tests. During the test, the displacement of the indenter has been controlled. The maximum depth limit was 2μm and peak hold time was 10 s. Indentation tests were carried out in five times and on a longitudinal section of weldment. The measured hardness shows a normal distribution and listed in Table 2. Due to larger grain size in the base material compared with the indentation depth (2μm), larger scattering of measured hardness were obtained. For the weldment material, the scatter band was smaller. Generally the hardness of weldment material is higher than base material.

Table 2. Measured indentation hardness

	Mean Value (GPa)	Standard Deviation
Base Material	3.48	0.53
Weldment material	3.10	0.33

3. Nano-indentation Simulation and Results

In order to determine the local stress-strain behavior of the weldment, nano-indentation technology was used. Through inverse analysis, the nano-indentation data can help to evaluate the elastoplastic properties of weldment.

3.1 FEM modeling

The indentation process was simulated in the commercial FEM code ABAQUS. Four-node axisymmetric elements were used in the simulation. Large strain feature was considered. Due to the

indenter was much stiffer than the test material, the indenter was considered as a perfect rigid and modeled as axisymmetric analytical rigid 140.6° cone, based on the equivalent contact area to depth ratio as a perfect Berkovich indenter. A reference point was defined to manipulate the translation of the indenter. The analysis was carried out under the displacement control without friction between the contact surfaces. Fig. 3 shows the mesh used in the analysis. The length of the whole mesh square is 30 micrometer. Finer meshes near the indenter were created to be able to describe the deformation and stress gradient below the indenter with sufficiently high accuracy. The base of the square was completely constrained, and the nodes along the center line were constrained in the horizontal direction due to axi-symmetry.

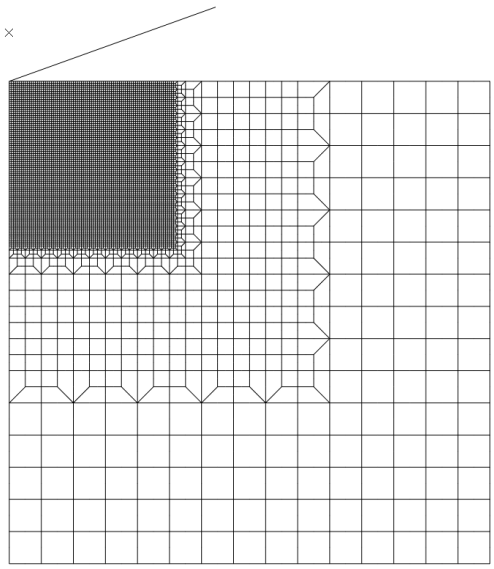

Figure 3. Mesh used in the finite element simulations

3.2 Elastoplastic material model

Due to the negligible heat affect zone, the fusion zone was assumed isotropic and homogeneous. A one-dimensional constitutive relation for the linear elastic, power law plastic material indicated in Eq. 1 was applied to describe the stress-strain relationship,

$$\sigma = \begin{cases} E\varepsilon, \sigma \le \sigma_{\mathrm{y}} \\ K\varepsilon^{n}, \sigma > \sigma_{y} \end{cases}, \tag{1}$$

where parameter σ_{y} is the initial yield stress, E represents the Young's modulus, K is the strain hardening coefficient and n is the strain hardening exponent. Young's modulus can be evaluated based on Oliver and Pharr method [3]. Through adjusting these input material parameters, different load-displacement curves can be obtained from finite element simulation. By comparing FE load-displacement curves with the experimental one, the best match should represent the correct input of material parameters, as shown in Fig. 7.

3.3 Simulation results

Fig. 4a shows the Mises stress distribution at indentation depth 1.94 μm. The stresses in the right part of the sample square are nearly zero, which means that the dimension of the sample square is enough and the boundary effect could be neglected. After unloading as shown in Fig. 4b, compression residual stresses could be found beneath the indenter tip.

As shown in Fig. 5, a load-displacement curve obtained by inverse nano-indentation analysis was compared with the measured load-displacement curves. Using the assumed linear elastic, power law plastic model, the simulated load-displacement curve cannot exactly match the shape of test curve. Simulated curve intersects with test curves, lower in small indentation depth and higher in large. The maximum load predicted matches that of experiment to within 5%.

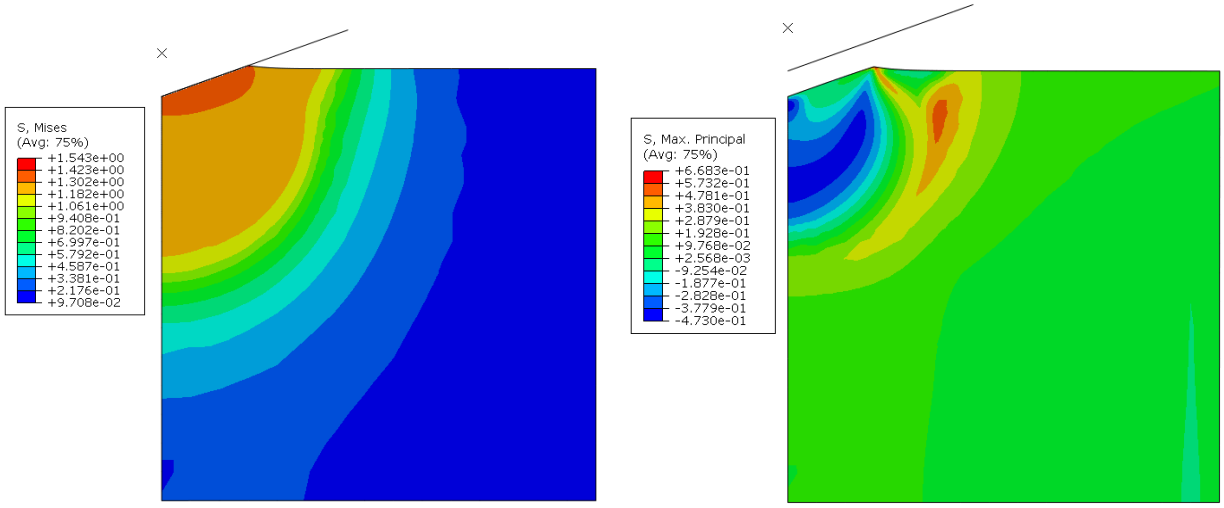

(a) (b)

Figure 4. Mises stress distribution under loading (a) and unloading (b) conditions.

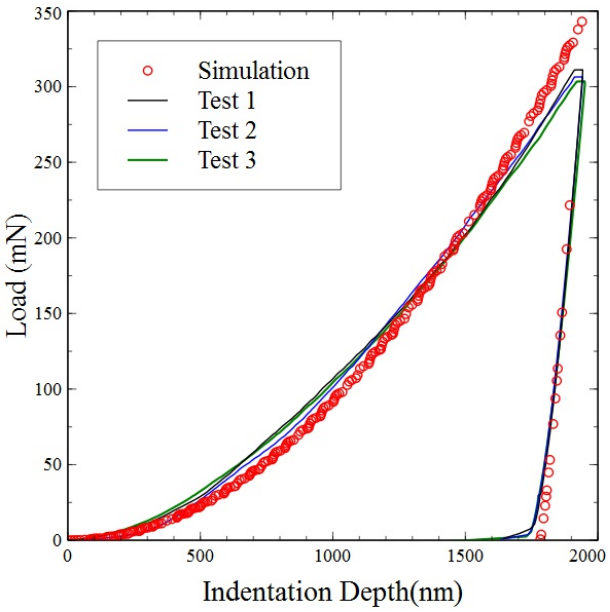

Figure 5. Comparison of load-displacement curves

3.3 Tensile test verification

Because of irregular weldment shape and narrow width, the weldment material properties cannot be obtained from a simple tension test. The nominal tensile curve of the welded specimen was determined from the uniaxial tension. The nominal strain was measured based on gauge length l_0=12mm. Using of the weldment material parameters indentified from the nano-indentation, FE simulations for the tensile test were carried. Comparison between the experiment and computation is shown in Fig. 6.

A quarter symmetry model was built for computation of local stresses and strains. Due to material difference between base metal and weldment, strains and stresses can be discontinuous on the fusion boundary. Maximum effective plastic strain at the 1250MPa nominal loading stress appears in the center of the weldment, while the maximum Mises stress on the maximal loading is localized on the fusion boundary. This coincides with the test, in which the plastic deformation occurs on the weldment. A comparison of nominal stress-strain curves between FEM simulation results with the experiment was carried out in Fig. 6. Calculated nominal strain was determined based on the initial gauge length of 12mm. A good correlation was obtained. The elastic moduli from base material, weldment material are nearly the same as the nominal behavior. Due to different yield stress of welding material, the nominal yield tensile stress is lower than base material. Yield will first occur in the weldment.

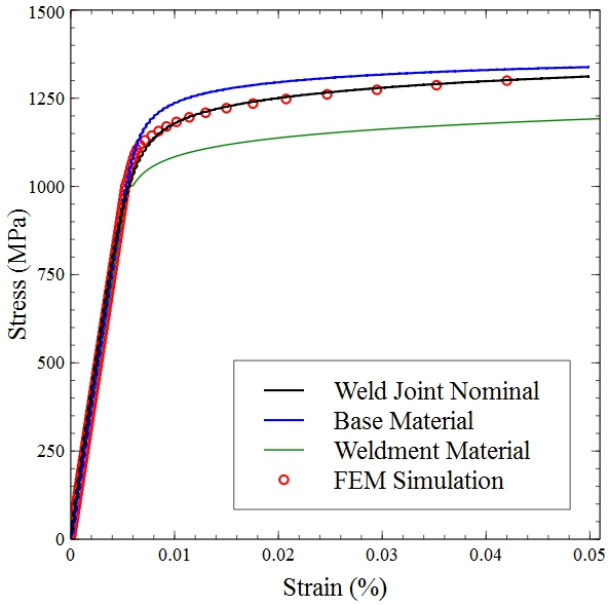

Figure 6. Comparison of tensile stress-strain curves.

4. Fatigue Life Prediction

4.1 Extended Cruse-Meyer model

The Cruse-Meyer model [15] includes both cyclic strain range $\Delta\varepsilon$ and mean stress σ_m as variable for predicting fatigue life in an explicit power law form for the uniaxial loading,

$$N_f = A\Delta\varepsilon^B 10^{C\sigma_m}, \tag{2}$$

where *A, B, C* are specific model parameters, σ_m is the mean stress, N_f is the number of cycles to failure, $\Delta\varepsilon$ is the strain amplitude. The Cruse-Meyer model is simple and practical for engineering application due to its explicit expression form.

The model can be extended to multiaxial fatigue by combining it with the critical plane concept. This critical plane concept postulates that fatigue cracks initiate and grow on certain planes where the material is mostly damaged [16]. Taking the concept of the Cruse-Meyer model, material failure under stress multiaxial state is described by the maximum normal strain range and the mean normal

stress acting on the maximum normal strain range plane. The extended Cruse-Meyer model is expressed as

$$N_f = A(\Delta\varepsilon_{\max})^B 10^{C\sigma_{n,mean}}. \quad (3)$$

Obviously, this equation is identical with the original Cruse-Meyer model.

In this work the parameters A and B are from the fitting of local strain-life curve of weldment at R = -1. And parameter C can be estimated at R = 0.1. In order to obtain the local stress and strain, FE computations were conducted for cyclic loadings with isotropic hardening assumed. Material properties were from previous analysis. Fig. *7* presents comparison between the predicted fatigue lifetime with the experimental results. All data are within the scatter band with a factor of 2.

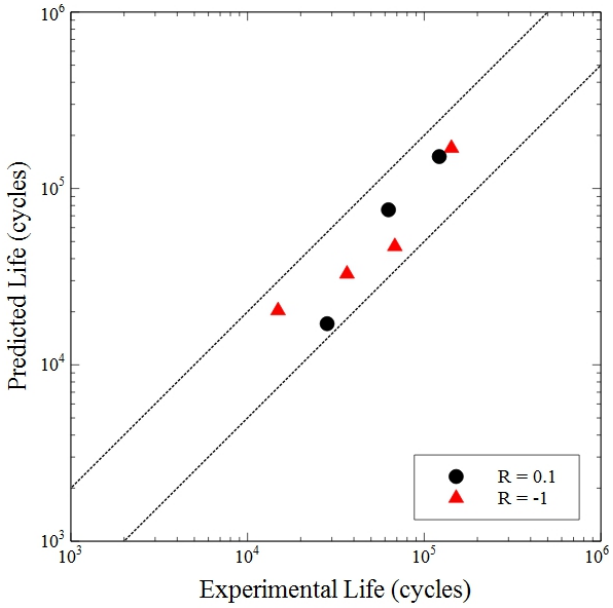

Figure 7. Fatigue life comparison results based on Cruse-Meyer model

4.2 Notched Fatigue Prediction

Even under uniaxial cyclic loading, the presence of a hole will cause a local multiaxial stress fields near the notch root, axial and circumferencial strresses. Below the root surface the stress state is general bi-axial tensile loading mode, although the axial tensile stress dominates. Additionally, the stresses and strains vary with the distance substantially. Hence, the multiaxial fatigue models find application to analyze the problem. The prediction from the extended Cruse-Meyer model is listed in Table 3, based on the local stresses and strains at the notch root surface. The parameters *ABC* are taken from the previous smooth fatigue analysis. Obviously, the prediction is too conservative in comparing with experiments.

Combining the extended Cruse-Meyer model with the critical distance method should improve the prediction. Two criteria, i.e. PM based and LM based, can be defined as

$$N_{p,d} = [A(\Delta\varepsilon_{\max})^B 10^{C\sigma_{n,mean}}]_d, \quad (4)$$

$$N_{p,l} = \frac{1}{l}\int_0^l A(\Delta\varepsilon_{\max})^B 10^{C\sigma_{n,mean}} . \quad (5)$$

One key issue in the critical distance method is determining the critical distance, *d*. Until now there is no effective method except searching to determine the critical distance for elasto-plastic problem. The most popular method is to determine the distance by minimizing the deviations between prediction and experiments. For instance, one may use the least square method to minimize $||N_{p,d}-N_f||$ or $||N_{p,l}-N_f||$ and to find the most appropriate distance. It follows that the critical distance for the PM is 0.437mm and 0.7mm for the LM. Generally, one may assume that the distance should be independent of loading ratio and temperature.

Table 3 lists the results for Cruse-Meyer PM and LM models. Results confirm significant improvement in predictions, in comparing with prediction results at root surface. The critical distance concept introduces a new variable into the model and makes it more flexible. However, applicability of it needs more detailed experimental and computational efforts. From the results we can observe LM predicted a little better than PM.

Table 3. Notched fatigue life comparison results

Notched Specimen No.	Experimental Life (cycles)	Predicted Life (cycles)		
		Root Surface	PM, d=0.437mm	LM, l=0.7mm
1	16201	923	12351	12450
2	31248	2439	44232	38132

5. Conclusions

It's been shown that the strength of Inconel 718 EB weldment is lower than that of the base metal, the weldment material properties cannot be obtained from simple tension test. Nano-indentation tests are useful to investigate the mechanical properties of weld joint. By assuming a power law plastic model, the elastoplastic properties of weldment material were derived from inverse nano-indentation analysis with help of finite element simulation. To verify the results, a comparison of nominal stress-strain curve between calculated and test results was carried out. The accuracy of the results is satisfactory.

To predict the fatigue life of weldment, the simple Cruse-Meyer model was extended to multiaxial fatigue directly and applied for this prediction. The predicted smooth fatigue lives were found to agree with the experimental data. Combining it with the critical distance concept provides a reasonable prediction for notched specimen fatigue. The basic assumption here is that the critical distance should be constant for the specific material and fatigue model which has to be verified further. Empirical determination of the critical distance needs to be refined.

References

[1] H. Schultz. Electron beam welding. Abington publishing, Cambridge, 1993.
[2] A.C. Fischer-Cripps, Nanoindentation. Vol. 1. Springer, 2011.
[3] W.C. Oliver, G.M. Pharr, An improved technique for determining hardness and elastic modulus using

load and displacement sensing indentation experiments. Journal of Materials Research, 7(1992) 1564-1583.
[4] S. Kucharski, Z. Mróz, Identification of yield stress and plastic hardening parameters from a spherical indentation test, International Journal of Mechanical Sciences, 49(2007) 1238-1250.
[5] J.A. Bannantine, J.J. Comer, J.L. Handrock, Fundamentals of metal fatigue analysis. Upper Saddle River, New Jersey: Prentice Hall, 1990.
[6] R.E. Peterson, Analytical approach to stress concentration effects in aircraft materials. In: Proceedings of the WADC Symposium on Fatigue of Metals. U.S. Air Force, Dayton, OH, USA, 1959.
[7] H. Neuber, Theoretical calculation of strength at stress concentration, Czech. J. Phys., 19(1996) 400.
[8] E. Siebel, M. Stieler, Dissimilar stress distributions and cyclic loading(in german). Z.VDI, 1997.
[9] David Taylor, The theory of critical distances, Elsevier, 2007.
[10] L. Susmel, D. Taylor, A novel formulation of the theory of critical distances to estimate lifetime of notched components in the medium-cycle fatigue regime. Fatigue Fract Eng Mater Struct 30(2007) 567–81.
[11] L. Susmel, D. Taylor, On the use of the theory of critical distances to estimate fatigue strength of notched components in the medium-cycle fatigue regime. In: Proceedings of FATIGUE 2006 Atlanta, USA.
[12] L. Susmel, Modified Wöhler curve method, theory of critical distances and Eurocode 3: A novel engineering procedure to predict the lifetime of steel welded joints subjected to both uniaxial and multiaxial fatigue loading, International Journal of Fatigue, 30(2008) 888-907.
[13] F. C. Campbell, Elements of metallurgy and engineering alloys. ASM International (OH), 2008.
[14] D.W. Worthem, D.F. Socie, Inhomogeneous deformation in INCONEL 718 during monotonic and cyclic loadings. Metallurgical and Materials Transactions A, 21 (1990) 3215–3220.
[15] T. Cruse, S. Mahadevan, R. Tryon, Fatigue reliability of gas turbine engine structures, NASA Contractor Report NASA/CR-97-206215,1997.
[16] M.W. Brown, K.J. Miller, A theory for fatigue under multiaxial stress-strain conditions. Proceeding of the Institution of Mechanical Engineers, 187(1973) 745-755.